

## Supplementary Information for article

### *Optical and scintillation properties of hybrid manganese(II) halides with formamidinium and acetamidinium cations*

Sergey A. Fateev<sup>a</sup>, Vladislava Y. Kozhevnikova<sup>d</sup>, Kirill M. Kuznetsov<sup>a</sup>, Daria E. Belikova<sup>a</sup>, Victor N. Khrustalev<sup>b, c</sup>, Eugene A. Goodilin<sup>a, d</sup> and Alexey B. Tarasov<sup>\*a, d</sup>

<sup>a</sup> Laboratory of New Materials for Solar Energetics, Department of Materials Science, Lomonosov Moscow State University; 1 Lenin Hills, 119991, Moscow, Russia;

<sup>b</sup> Inorganic Chemistry Department, Peoples' Friendship University of Russia (RUDN University), 6 Miklukho-Maklay Str., 117198, Moscow, Russia

<sup>c</sup> N.D. Zelinsky Institute of Organic Chemistry RAS, 47 Leninsky Prosp., 119991, Moscow, Russia

<sup>d</sup> Department of Chemistry, Lomonosov Moscow State University; 1 Lenin Hills, 119991, Moscow, Russia

\*corresponding author e-mail: [alexey.bor.tarasov@yandex.ru](mailto:alexey.bor.tarasov@yandex.ru).

Table S1. Parameters of the crystal structure refinement.

Phase	<b>Ac<sub>2</sub>MnBr<sub>4</sub></b>	<b>FA<sub>3</sub>MnBr<sub>5</sub></b>	<b>(i-PrOH)<sub>4</sub>MnBr<sub>2</sub></b>
<b>Empirical formula</b>	C <sub>4</sub> H <sub>14</sub> Br <sub>4</sub> MnN <sub>4</sub>	C <sub>3</sub> H <sub>15</sub> Br <sub>5</sub> MnN <sub>6</sub>	C <sub>12</sub> H <sub>32</sub> Br <sub>2</sub> MnO <sub>4</sub>
<b>M, g/mol</b>	492.73	589.65	455.12
<b>Crystal system</b>	Triclinic	Orthorombic	Monoclinic
<b>Space group</b>	<i>P</i> $\bar{1}$	<i>Pnma</i>	<i>P2</i> <sub>1</sub> / <i>c</i>
<b>a, Å</b>	7.87110(7)	11.2782(4)	5.78966(8)
<b>b, Å</b>	7.97838(9)	15.3630(4)	10.52718(16)
<b>c, Å</b>	12.90853(12)	9.5551(2)	16.74863(19)
<b>α, deg.</b>	72.6600(9)	90	90
<b>β, deg.</b>	78.5236(7)	90	97.3885(12)
<b>γ, deg.</b>	67.0044(10)	90	90
<b>V, Å<sup>3</sup></b>	709.158(14)	1655.58(8)	1012.33(2)
<b>Z</b>	2	4	2
<b>D (calc), g/cm<sup>3</sup></b>	2.307	2.366	1.493
<b>μ, mm<sup>-1</sup></b>	20.549	20.517	9.980
<b>F(000)</b>	462	1100	462
<b>Crystal size, mm</b>	0.18×0.05×0.04	0.34×0.24×0.22	0.10×0.10×0.10

<b><math>\Theta</math> range for data collection, deg.</b>	3.603 – 77.991	3.88 – 77.58	4.974 – 77.759
<b>Index ranges</b>	$-9 \leq h \leq 9$ $-10 \leq k \leq 9$ $-16 \leq l \leq 16$	$-14 \leq h \leq 13$ $-17 \leq k \leq 19$ $-8 \leq l \leq 12$	$-7 \leq h \leq 7$ $-13 \leq k \leq 12$ $-21 \leq l \leq 20$
<b>Reflections collected/independent</b>	93076/3004	9286/1772	11458/2139
<b><math>R_{\text{int}}</math></b>	0.0850	0.0978	0.0413
<b>Reflections with <math>I &gt; 2\sigma(I)</math></b>	3001	1705	2001
<b>Goodness-of-fit on F</b>	1.057	1.014	1.076
<b>Final R indices [<math>I &gt; 2\sigma(I)</math>]</b>	$R_1 = 0.0306$ $wR_2 = 0.0826$	$R_1 = 0.0448$ $wR_2 = 0.1100$	$R_1 = 0.0268$ $wR_2 = 0.0601$
<b>R indices (all data)</b>	$R_1 = 0.0306$ $wR_2 = 0.0827$	$R_1 = 0.0466$ $wR_2 = 0.1117$	$R_1 = 0.0297$ $wR_2 = 0.0613$
<b><math>T_{\text{min}} / T_{\text{max}}</math></b>	0.036 / 0.404	0.006 / 0.084	0.352 / 1.000
<b>Largest diff. peak/hole, <math>e/\text{\AA}^3</math></b>	1.689/-0.879	1.137/-0.609	0.520 / -0.445

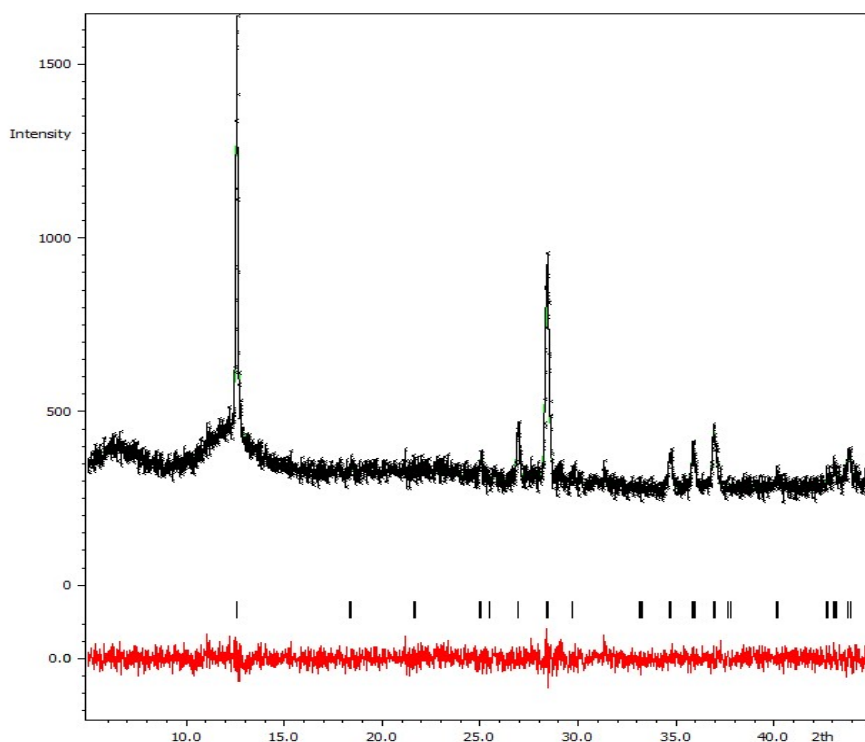


**Figure S1.** X-ray powder pattern fitting for  $\text{FAMnBr}_3$ . The observed and calculated patterns are shown by black dots and green solid line respectively. The vertical marks show positions calculated for Bragg

reflections. The red trace on the bottom is a plot of the difference between calculated and observed intensities.

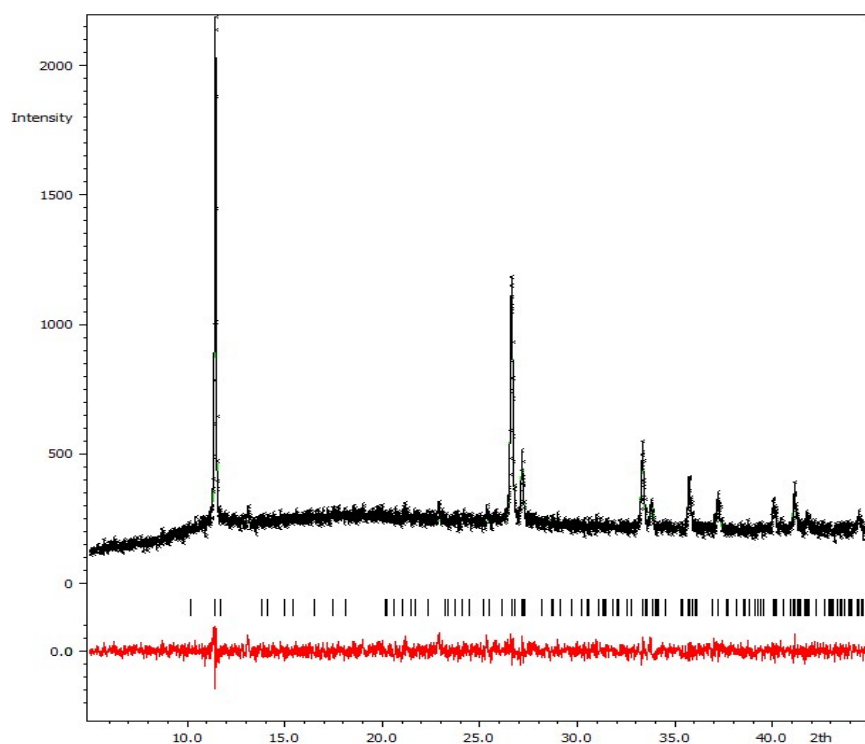


**Figure S2.** X-ray powder pattern fitting for  $\text{AcMnBr}_3$ . The observed and calculated patterns are shown by black dots and green solid line respectively. The vertical marks show positions calculated for Bragg reflections. The red trace on the bottom is a plot of the difference between calculated and observed intensities.

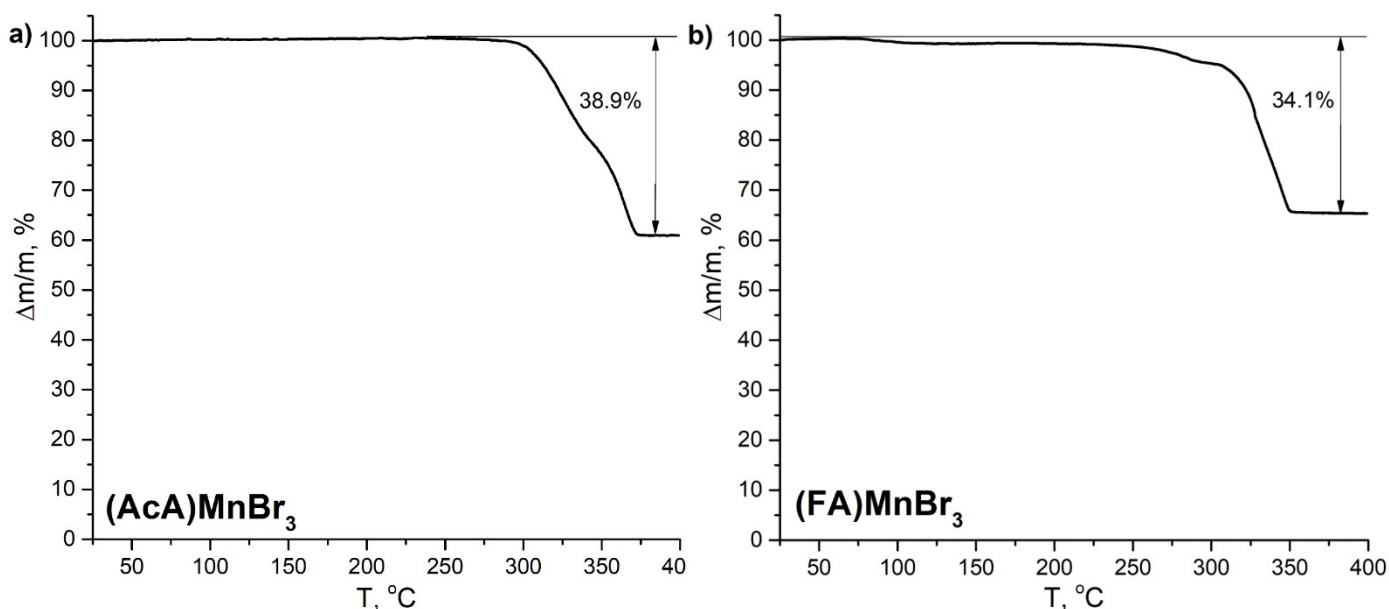


**Figure S3.** TG mass loss curve of the  $(\text{FA})\text{MnBr}_3$  and  $(\text{AcA})\text{MnBr}_3$ .

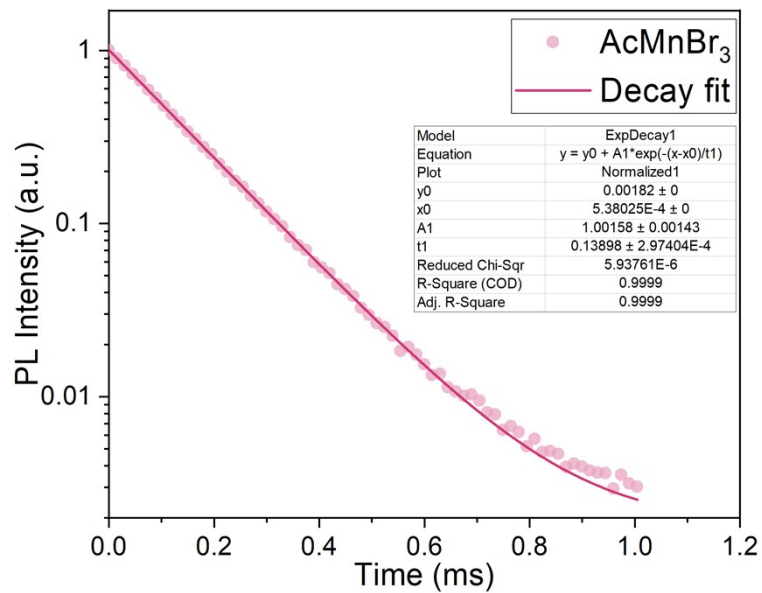


**Figure S4.** Fitted PL decay curve of the AcMnBr<sub>3</sub> powder.

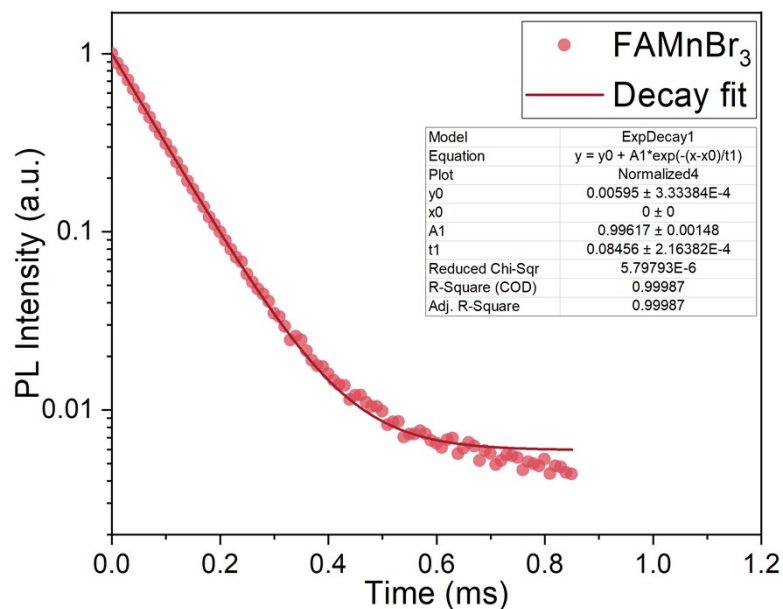


**Figure S5.** Fitted PL decay curve of the FAMnBr<sub>3</sub> powder.

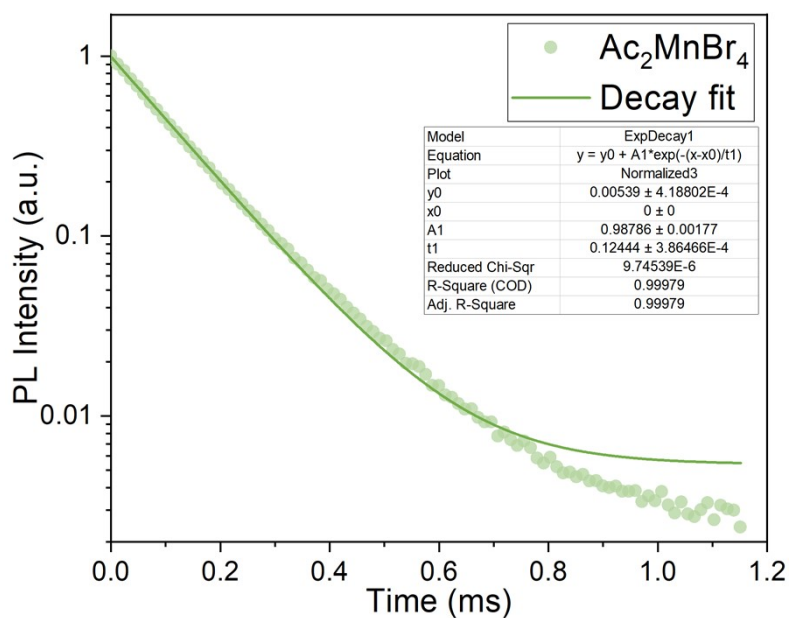


**Figure S6.** Fitted PL decay curve of the Ac<sub>2</sub>MnBr<sub>4</sub> powder.

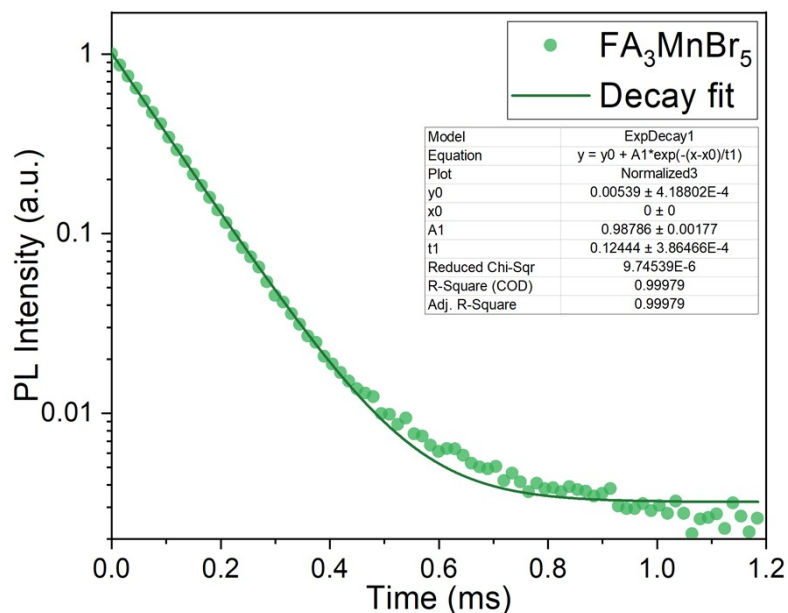


**Figure S7.** Fitted PL decay curve of the FA<sub>3</sub>MnBr<sub>5</sub> powder.

**Table S2.** Optical properties of the studied phases: photoluminescence excitation maxima (PLE<sub>max</sub>), photoluminescence maxima (PL<sub>max</sub>), fullwidth at half maximum (FWHM), Stokes shift, photoluminescence quantum yields (PLQY) and photoluminescence decay times ( $\tau$ ).

Phase	PLE <sub>max</sub> , nm/eV	PL <sub>max</sub> , nm/eV	FWHM, nm/meV	Stokes Shift, nm/eV	PLQY, %	$\tau$ , $\mu$ s
AcMnBr <sub>3</sub>	372/3.33	660/1.88	97/279	120/1.45	43	139.0
FAMnBr <sub>3</sub>	373/3.32	654/1.90	94/262	118/1.42	4	84.6
Ac <sub>2</sub> MnBr <sub>4</sub>	272/4.56	525/2.36	52/249	72/2.2	21	126.4
FA <sub>3</sub> MnBr <sub>5</sub>	277/4.48	518/2.39	53/264	63/2.09	7	96.7